Abbreviated Gadoxetic Acid-Enhanced MRI for the Detection of Liver Metastases in Patients With Potentially Resectable Pancreatic Ductal Adenocarcinoma

Yamaguchi, Takeru ; Sofue, Keitaro ; Ueshima, Eisuke ; Ueno, Yoshiko ; Tsujita, Yushi ; Yabe, Shinji ; Shirakawa, Sachiyo ; Toyama, Hirochika…

(Citation)
Journal of Magnetic Resonance Imaging,56(3):725-736

(Issue Date)
2022-09

(Resource Type)
journal article

(Version)
Accepted Manuscript

(URL)
https://hdl.handle.net/20.500.14094/0100477338

Abbreviated Gadoxetic Acid-enhanced MRI for the Detection of Liver Metastases in Patients with Potentially Resectable Pancreatic Ductal Adenocarcinoma

- Research Article-

Abstract

Background: Gadoxetic acid-enhanced MRI is useful in detecting liver metastases from pancreatic ductal adenocarcinoma (PDAC). However, the long examination time limits its utility in the initial workup of patients with PDAC.

Purpose: To evaluate the incremental value of an abbreviated gadoxetic acid-enhanced MRI for the detection of liver metastases in patients with PDAC.

Study Type: Retrospective

Population: Patients (*n*=130) with potentially resectable PDAC (women, 58 [44.6%]).

Field Strength/Sequence: 1.5T and 3T; gradient dual-echo T1-weighted (in-phase and opposed-phase), fat-suppressed fast spin-echo T2-weighted, single-shot echo-planar diffusion-weighted, and three-dimensional fat-suppressed T1-weighted gradient-echo dynamic contrast-enhanced and hepatobiliary phase sequences, as well as contrast enhanced computed tomography (CECT).

Assessment: Three radiologists independently reviewed three different image sets to detect liver metastases: set 1, CECT alone; set 2, CECT and abbreviated MRI comprising fat-suppressed T2-weighted, diffusion-weighted, and hepatobiliary phase images; and set 3, CECT and standard gadoxetic acid-enhanced MRI.

Statistical Tests: Figure of merit (FOM) was compared using the jackknife alternative free-response receiver operating characteristics, and other per-lesion and per-patient diagnostic

parameters for each image set were compared using McNemar's and Fisher's test. $P<.05$ was considered statistically significant.

Results: A total of 43 liver metastases were identified in 13 patients. Reader-averaged FOM to detect liver metastases were significantly higher for sets 2 (0.884) and 3 (0.886) than for set 1 (0.609), while they were comparable between sets 2 and 3 ($P=.96$). The mean per-patient sensitivities, negative predictive values, and accuracies were significantly higher for sets 2 and 3 than for set 1, while those between sets 2 and 3 were not significantly different (not applicable, $P>.99$, and $P>.99$, respectively).

Data Conclusion: Gadoxetic acid-enhanced MRI combined with CECT had higher diagnostic performance than CECT alone for the detection of liver metastases in patients with PDAC. The incremental values were comparable for the abbreviated MRI and standard MRI.

Keywords: Pancreatic Adenocarcinoma, Liver Metastases, MRI, Gadolinium Ethoxybenzyl DTPA

Introduction

Pancreatic ductal adenocarcinoma (PDAC) is the fourth leading cause of cancer-related deaths in the United States, making it a major public health concern (1). Surgical resection is the only potentially curative treatment for PDAC. Approximately half of the patients with PDAC present with metastatic diseases, most commonly with liver metastases (2, 3). In these patients, the detection and accurate diagnosis of liver metastases are crucial because their presence results in substantial changes in the treatment strategy (4). The National Comprehensive Cancer Network guidelines recommend dynamic contrast-enhanced computed tomography (CECT) as the preferred imaging modality for the initial evaluation of local resectability and detection of metastases in patients with PDAC (4). Endoscopic ultrasonography and endoscopic retrograde cholangiopancreatography are subsequently performed to confirm the diagnosis. MRI is not routinely used for staging mainly because of the limited throughput and its limited availability (4).

Gadoxetic acid-enhanced MRI enables the acquisition of hepatobiliary phase (HBP) images and has been reported to be useful in detecting liver metastases in patients with PDAC, with better sensitivity than that of CECT (5, 6). However, the long examination time may limit the use of gadoxetic acid-enhanced MRI for patients with PDAC. Abbreviated MRI protocols with limited sequences, which can theoretically be performed in a shorter examination time than the conventional protocols, could be a solution to this problem. Abbreviated MRI protocols that include T2-weighted (T2W), diffusion-weighted (DW), and HBP images have been recently shown to be highly accurate for the detection and characterization of liver metastases from colorectal cancer and neuroendocrine tumors (7–9). Abbreviated MRI protocols may improve the throughput and availability of MRI examinations without compromising the diagnostic performance, which would help in the

initial workup and accurate decision-making regarding the therapeutic strategy for patients with PDAC.

Thus, the purpose of our study was to evaluate the incremental diagnostic value of an abbreviated gadoxetic acid-enhanced MRI for the detection of liver metastases in patients with PDAC.

Materials and Methods

Study Design and Population

This retrospective, single-institution study was approved by the institutional review board. The need for informed consent was waived owing to the retrospective nature of the study. Overall, 341 consecutive patients with pathologically proven PDAC who underwent both CECT and gadoxetic acid-enhanced MRI between June 2014 and March 2020, were eligible. The exclusion criteria were PDAC recurrence after surgery (n = 7), receiving neoadjuvant chemotherapy (n = 39), pathology other than PDAC (n = 3), locally unresectable PDAC according to the National Comprehensive Cancer Network guidelines (n = 19), more than 10 liver lesions (n = 9), and no adequate imaging follow-up (i.e., follow-up for < 6 months, n = 134). Finally, 130 patients (72 men and 58 women) with a mean age 68.7 ± 10.7 years were included in the analysis (Fig. 1).

CT Examination

Multiphasic CECT scans were obtained with multi-detector row CT scanners (Aquilion 64 (n = 88), One (n = 16), or Precision (n = 6), Canon Medical Systems; and

SOMATOM Force (*n* = 20), Siemens Healthcare). An iodinated contrast material was injected into an antecubital vein using a mechanical power injector at a dose of 600 mgI/kg body weight with a fixed duration of 30 s. Multiphasic CT images consisted of unenhanced, early arterial (18–23 s), pancreatic (38–45 s), portal venous (70 s), and equilibrium (180 s) phase images. All multiphasic images were reconstructed with 5 mm slice thickness, and the pancreatic phase and portal venous phase images were also reconstructed with 0.5–0.6 mm slice thickness. A bolus-tracking technique was used to obtain early arterial phase images immediately after the trigger threshold was achieved. The acquisition and reconstruction parameters for the CT scanners are presented in Table 1.

MRI Examination

Gadoxetic acid-enhanced MRI examinations were performed on various MR scanners (Ingenia 3T (*n* = 46), Achieva 3T (*n* = 35), and Achieva 1.5T (*n* = 13), Philips Medical Systems; Titan 3T (*n* = 36), Canon Medical Systems). The baseline MRI examinations included breath-hold gradient dual-echo T1-weighted (in-phase and opposed-phase), fat-suppressed fast spin-echo T2W, DW (b=0, 500, and 1000 s/mm^2, applied in three orthogonal directions), dynamic contrast-enhanced, and HBP sequences. Dynamic contrast-enhanced and HBP sequences were obtained using a 3D fat-suppressed T1-weighted spoiled gradient-recalled echo pulse sequence. After obtaining precontrast images, gadoxetic acid (Primovist, Bayer Pharma) was intravenously administered (0.025 mmol/kg body weight; 1 mL/s), followed by a 20-mL saline flush. Consequently, postcontrast images were obtained during the arterial phase (27–40 s using the fluoroscopic triggering technique), portal venous phase (70 s), and transitional phase (120 s). HBP images were acquired 20 min after the contrast administration. All the pulse sequence parameters are summarized in Table 2.

Image Analysis

Three radiologists (K.S., E.U., and Y.U. with 19, 15, and 14 years of experience in abdominal imaging, respectively) independently reviewed the following three image sets to detect liver metastases: set 1, CECT consisting of unenhanced, pancreatic, portal venous, and equilibrium phase images; set 2, the combination of CECT and abbreviated gadoxetic acid-enhanced MRI consisting of fat-suppressed T2W, DW, and HBP images; and set 3, the combination of CECT and the standard gadoxetic acid-enhanced MRI consisting of all acquired sequence images. The abbreviated protocol followed previous studies which have reported that the protocol was highly accurate for the diagnosis of liver metastases from colorectal cancer (7, 9). The abbreviated MRI protocol was simulated by extracting the three sequences from the standard MRI protocol. Thus, the total examination time of the abbreviated MRI protocol was estimated as less than 10 min, while the standard MRI protocol took more than 30 min to be completed. Images were reviewed using a picture archiving and communication system. Readers were blinded to the patient's clinical information but were aware that the population had pathologically proven locally resectable or borderline resectable PDAC. Image interpretation consisted of two different reading sessions. In the first reading session, the readers reviewed set 1 followed by the review of set 2 for each patient. In the second reading session, readers reviewed set 3. Readers were allowed to refer to their own interpretation results of set 1 when they reviewed sets 2 and 3. To avoid recall bias, the two reading sessions were conducted with at least a 2-week interval, and the images of each patient were reviewed in a random order during each reading session.

The readers were asked to record all the focal liver lesions detected. For each lesion, the segmental location according to the Couinaud classification and the largest diameter on the axial plane with the corresponding slice number were recorded. The readers were asked to assess the probability of malignancy for each lesion based on a 5-point scale: 1 = definitely

benign, 2 = probably benign, 3 = indeterminate, 4 = probably malignant, and 5 = definitely malignant. On CECT, liver metastases were diagnosed when a lesion was hypoattenuated and less enhanced than the liver parenchyma with peripheral enhancement. On MRI, liver metastases were diagnosed when a lesion showed irregular or ill-defined borders, hypointensity on T1-weighted images, mild hyperintensity on T2W images, hypointensity in the HBP, hyperintensity on DW images not attributable to T2 shine-through, and peripheral enhancement on dynamic contrast-enhanced sequences (10).

Reference Standard

The reference standard for liver metastases was based on histopathologic findings (biopsy or resection) or all available imaging modalities, including CT and MRI. When information on the pathology was not available, (i) liver lesions on CT or MRI with characteristics indicative of metastases and (ii) either a size increase on follow-up imaging or size decrease following chemotherapy were considered metastases (11). Liver lesions that were stable for at least 6 months on imaging without evidence of metastases on intraoperative examination were considered benign. The study coordinator (T.Y. with 7 years of experience in abdominal imaging), who was not involved in the reading sessions, collected the clinical and histological data and was responsible for classifying all the lesions detected by the three readers into metastatic or benign lesions. In our institution, the multidisciplinary team including radiologists, surgeons, gastroenterologist, and oncologists discussed the treatment strategy for every patient with PDAC. For this study, two experienced radiologists (T.Y. and K.S. with 7 and 19 years of experience in abdominal radiology, respectively) reviewed all the CECT images again to determine the local resectability of the PDAC in consensus according to the National Comprehensive Cancer Network guidelines before the image analysis (4), and a surgeon (H.T. with 20 years of experience) confirmed the results of the review.

Statistical Analysis

Continuous variables were summarized as the mean ± standard deviation, while categorical variables were presented as counts and frequencies. Inter-reader agreement was calculated using Fleiss κ statistics for each image set based on the scores of true-positive and false-positive lesions. The results were stratified qualitatively by scores (0.01–0.20, slight; 0.21–0.40, fair; 0.41–0.60, moderate; 0.61–0.80, substantial; and 0.81–0.99, almost perfect) (12). Fleiss κ statistics were performed using the IBM SPSS Statistics software for Windows version 20 (IBM Corp., Armonk, NY).

To evaluate and compare the diagnostic performance of each image set, receiver operating characteristic analysis was performed using jackknife alternative free-response operating characteristic (JAFROC) software (JAFROC, version 4.2.1; http://www.devchakraborty.com) (13). Figure of merit (FOM), defined as the probability that a lesion is rated higher than the highest-rated non-lesions on normal images (14), was used to indicate the overall diagnostic performance.

The per-lesion sensitivity and positive predictive value (PPV) of each image set for the detection of liver metastasis were calculated, with positive liver metastasis defined as scores of 4–5. Per-patient sensitivity, specificity, PPV, negative predictive value, and accuracy were also determined, considering that a patient with at least one lesion scored 4 or 5 was positive for liver metastasis. McNemar's test was used to compare sensitivities, specificities, and accuracies, and Fisher's exact test was used to compare the PPVs and negative predictive values among the three image sets. McNemar's test and Fisher's exact test were performed using MedCalc software version 20 (MedCalc Software, Ostend, Belgium). A two-sided *P* value less than .05 was considered statistically significant.

Results

Characteristics of the Patients and Liver Metastases

A total of 43 metastases were detected in 13 of the 130 patients (10.0%). The characteristics of the patients and the liver metastases are provided in Table 3. Out of the 130 patients, 101 patients (77.7%) had resectable PDAC, and the other 29 patients (22.3%) had borderline resectable PDAC. The mean diameter of liver metastases was 6.3 mm (range, 3.1–13.2 mm), and 38 metastases (88.4%) measured less than 10 mm in diameter. Among the 43 lesions, the reference standard was obtained by the pathological analysis of 7 (16.3%) lesions and follow-up imaging examinations of the remaining 36 (83.7%) lesions. The mean time interval between the acquisition of CECT images and gadoxetic acid-enhanced-MRI was 9.2 days (range, 0–54 days), and CECT was performed before gadoxetic acid-enhanced-MRI in 111 (85.4%) patients.

Per-lesion Diagnostic Performance

The readers detected on average 263, 322, and 322 focal liver lesions including both benign and malignant lesions for sets 1, 2, and 3, respectively (Fig. 2). Inter-reader agreement was substantial ($\kappa = 0.79$ [95% CI: 0.64, 0.93]), moderate ($\kappa = 0.46$ [95% CI: 0.31, 0.60]), and moderate ($\kappa = 0.41$ [95% CI: 0.33, 0.49]) for sets 1, 2, and 3, respectively.

FOMs from the JAFROC analysis of each imaging set for each reader are summarized in Table 4. The reader-averaged FOMs determined by the mean value of the JAFROC analysis were 0.609, 0.884, and 0.886 for sets 1, 2, and 3, respectively. The 95% confidence intervals for the difference in FOM were 0.175–0.375 for set 1 and set 2, 0.177–0.378 for set

1 and set 3, and -0.103–0.098 for set 2 and set 3. JAFROC analysis indicated that the reader-averaged FOMs were significantly different between sets 1 and 2 and between sets 1 and 3, whereas they were comparable between sets 2 and 3 ($P = .96$).

The mean per-lesion sensitivities in the detection of liver metastases were 24.8%, 81.4%, and 83.7% for sets 1, 2, and 3, respectively. The per-lesion sensitivities of sets 2 and 3 were significantly higher than those of set 1 for each reader and the mean (Table 4). Meanwhile, there was no significant difference in sensitivity between sets 2 and 3 for each reader and the mean ($P = .50$, $P > .99$, $P > .99$, and $P = .51$ for readers 1, 2, 3, and the mean). The mean per-lesion PPVs were 76.2%, 86.1%, and 85.7% for sets 1, 2, and 3, respectively. There was no significant difference in the PPV between each pair of image sets for each reader and the mean (reader 1, $P = .21$, $P = .20$, and $P > .99$; reader 2, $P > .99$, $P = .72$, and $P = .30$; reader 3, $P = .44$, $P = .06$, and $P = .26$; the mean, $P = .15$, $P > .16$, and $P > .99$ for set 1 vs. 2, set 1 vs. 3, and set 2 vs. 3, respectively) (Table 4).

Five, 13, and 12 lesions were incorrectly diagnosed as malignant by at least one reader in set 1, 2, and 3. All of the 5 false positive lesions in set 1 were hypoattenuating relative to liver parenchyma, but hyperattenuating relative to cerebrospinal fluid. Out of the 16 false positive lesions in set 2 or 3, 13 lesions (81%) showed hyperintensity on diffusion weighted images.

Per-patient Diagnostic Performance

The per-patient diagnostic performance is shown in Table 5. The mean per-patient sensitivities, negative predictive values, and accuracies of sets 2 and 3 were significantly higher than those of set 1, while those between sets 2 and 3 were not significantly different (not applicable, $P > .99$, and $P > .99$, respectively). The mean per-patient specificities and PPVs were comparable among the three image sets (specificity, $P > .99$, $P > .99$, and $P > .99$;

PPV, $P = .09$, $P = .09$, and $P > .99$ for set 1 vs. 2, set 1 vs. 3, and set 2 vs. 3, respectively). Compared with set 1, 9 (6.9%), 7 (5.4%), and 5 (3.8%) additional patients for set 2, and 9 (6.9%), 5 (3.8%), and 7 (5.4%) additional patients for set 3 were correctly diagnosed by readers 1, 2, and 3, respectively (Fig. 3 and 4). Among the patients who were identified as having indeterminate liver lesions (score 3) in set 1, 69.2% (27/39), 61.5% (16/26), and 66.7% (18/27) were diagnosed as not having liver metastases with higher confidence (score 1 or 2) in set 2, and 74.4% (29/39), 69.2% (18/26), and 74.1% (20/27) in set 3 (Fig. 5).

Discussion

The usefulness of an abbreviated MRI protocol for the initial workup of PDAC remains unclear. We found that the combination of CECT and gadoxetic acid-enhanced MRI provided significantly higher diagnostic performance than CECT alone for the detection of liver metastases in potentially resectable PDAC. The incremental value of an abbreviated MRI protocol comprising T2-weighted, diffusion-weighted, and hepatobiliary phase imaging was comparable with that of the standard MRI protocol. These results suggest that an abbreviated MRI protocol can be a time-efficient alternative to the standard MRI protocol for the initial workup of PDAC.

The diagnostic performance of the combination of CECT and gadoxetic acid-enhanced MRI for liver metastases from PDAC in our study was in line with previous publications, with a reported sensitivity of 76–94% and PPV of 82–100% (5, 6, 15). Our results also revealed that an abbreviated or standard gadoxetic acid-enhanced MRI protocol can provide more accurate therapeutic decisions than CECT alone by detecting liver

metastases in patients with potentially resectable PDAC. The sensitivity of CECT in our study was substantially lower than that in a meta-analysis that reported a mean sensitivity of 45% for liver metastases in a total of 987 patients with PDAC (11). A possible reason for this discrepancy is that the majority of liver metastases in our study were smaller than 10 mm, because our study population included only locally resectable or borderline resectable PDAC (5, 16, 17). Another possible explanation is that the majority of CECT scans were performed before MRI, which can introduce disease progression bias because liver metastases from PDAC can rapidly progress (18).

In previous studies with a similar design including patients with colorectal cancer and neuroendocrine tumors, abbreviated MRI protocols that included T2W, DW, and HBP images were highly accurate for the detection and characterization of liver metastases (7–9). Similar results have also been reported for the detection of hepatocellular carcinomas (19–22), further supporting the effectiveness of abbreviated MRI protocols. The non-significant difference in FOM, sensitivity, and PPV between abbreviated MRI and standard MRI protocols is probably due to the inclusion of DW and HBP images. Several studies and meta-analyses have confirmed that these sequences have high detection capability, especially for small focal liver lesions (16, 23–25). Another possible reason is that multiphasic CECT was substituted for dynamic sequences of contrast-enhanced MRI in set 2 in our study (26).

An abbreviated MRI protocol could be implemented at a lower cost and with a shorter examination time than a standard gadoxetic acid-enhanced MRI protocol without compromising diagnostic performance. The proposed abbreviated MRI protocol composed of fast spin-echo T2W, DW, and HBP sequences has an estimated examination time of less than 10 min, assuming that patients undergo contrast administration outside the MRI suite and that all sequences are acquired approximately 10–20 min after contrast injection (27, 28). This amount of time could have been less than one-third of the time required for the standard MRI

protocol. With respect to cost saving, Canellas et al. reported that the cost of gadoxetic acid-enhanced MRI acquisition for colorectal liver metastasis surveillance can potentially be reduced by up to 40% by utilizing an abbreviated MRI protocol (7). The shorter examination time of an abbreviated MRI protocol may improve the throughput and availability of MR scanners, facilitating decision-making for treatment strategies in patients with PDAC.

Limitations

First, this was a retrospective study, and the abbreviated MRI protocol was simulated using a conventional MRI protocol, inevitably introducing recall bias. Although we set a 2-week interval between the two reading sessions to avoid recall bias, further prospective studies are necessary to confirm our findings. Second, only a limited number of patients with liver metastases (n = 13) were included. However, because the incidence of liver metastasis (10.0%) was in accordance with previous studies (6, 29, 30), we considered the number to reflect the real-world clinical setting. Third, a large number of cases were excluded, mainly due to a lack of adequate follow-up imaging, receiving neoadjuvant chemotherapy, and more than 10 liver lesions, which could have introduced a selection bias. Patients with more than 10 liver lesions were excluded since it is impractical to evaluate a myriad of hepatic cysts or metastases. Similar criteria were used in previous studies (7). An increasing number of patients with pancreatic adenocarcinoma are receiving neoadjuvant therapy nowadays, and we believe that further studies are necessary for this population. Finally, no histological confirmation was available for the majority of detected lesions. This reflects current clinical practice in which imaging examinations are generally used to diagnose liver metastasis, and biopsy or surgical resection is impractical. As the reference standard in our study followed the criteria recommended in a recently published meta-analysis (11), we believe this limitation is acceptable.

Conclusion

In conclusion, gadoxetic acid-enhanced MRI combined with CECT provided higher diagnostic performance than did CECT alone for the detection of liver metastases in patients with potentially resectable PDAC. The incremental value of the abbreviated MRI protocol was comparable to that of the standard MRI protocol. In conclusion, the abbreviated MRI protocol can be a reasonable non-invasive examination for the initial workup of patients with PDAC who are candidates for curative surgery.

References

1. Siegel RL, Miller KD, Fuchs HE, Jemal A. Cancer Statistics, 2021. CA Cancer J Clin 2021;71:7-33.

2. Kamisawa T, Isawa T, Koike M, Tsuruta K, Okamoto A. Hematogenous metastases of pancreatic ductal carcinoma. Pancreas 1995;11:345-9.

3. Saad AM, Turk T, Al-Husseini MJ, Abdel-Rahman O. Trends in pancreatic adenocarcinoma incidence and mortality in the United States in the last four decades; a SEER-based study. BMC Cancer 2018;18:688.

4. Tempero MA, Malafa MP, Al-Hawary M et al. Pancreatic Adenocarcinoma, Version 2.2021, NCCN Clinical Practice Guidelines in Oncology. J Natl Compr Canc Netw 2021;19:439-457.

5. Motosugi U, Ichikawa T, Morisaka H et al. Detection of pancreatic carcinoma and liver metastases with gadoxetic acid-enhanced MR imaging: comparison with contrast-enhanced multi-detector row CT. Radiology 2011;260:446-53.

6. Ito T, Sugiura T, Okamura Y et al. The diagnostic advantage of EOB-MR imaging over CT in the detection of liver metastasis in patients with potentially resectable pancreatic cancer. Pancreatology 2017;17:451-456.

7. Canellas R, Patel MJ, Agarwal S, Sahani DV. Lesion detection performance of an abbreviated gadoxetic acid-enhanced MRI protocol for colorectal liver metastasis surveillance. Eur Radiol 2019;29:5852-5860.

8. Hayoz R, Vietti-Violi N, Duran R, Knebel JF, Ledoux JB, Dromain C. The combination of hepatobiliary phase with Gd-EOB-DTPA and DWI is highly accurate for the detection and characterization of liver metastases from neuroendocrine tumor. Eur Radiol 2020;30:6593-6602.

9. Ghorra C, Pommier R, Piveteau A et al. The diagnostic performance of a simulated "short" gadoxetic acid-enhanced MRI protocol is similar to that of a conventional protocol for the detection of colorectal liver metastases. Eur Radiol 2021;31:2451-2460.

10. Danet IM, Semelka RC, Leonardou P, et al. Spectrum of MRI appearances of untreated metastases of the liver. AJR Am J Roentgenol. 2003;181:809-17.

11. Alabousi M, McInnes MD, Salameh JP et al. MRI vs. CT for the Detection of Liver Metastases in Patients With Pancreatic Carcinoma: A Comparative Diagnostic Test Accuracy Systematic Review and Meta-Analysis. J Magn Reson Imaging 2021;53:38-48.

12. Viera AJ, Garrett JM. Understanding interobserver agreement: the kappa statistic. Fam Med. 2005;37:360-3.

13. Chakraborty DP. Analysis of location specific observer performance data: validated extensions of the jackknife free-response (JAFROC) method. Acad Radiol 2006;13:1187-93.

14. Chakraborty DP, Berbaum KS. Observer studies involving detection and localization: modeling, analysis, and validation. Med Phys 2004;31:2313-30.

15. Tsurusaki M, Numoto I, Oda T et al. Assessment of Liver Metastases Using CT and MRI Scans in Patients with Pancreatic Ductal Adenocarcinoma: Effects of Observer Experience on Diagnostic Accuracy. Cancers (Basel) 2020;12:1455.

16. Tsurusaki M, Sofue K, Murakami T. Current evidence for the diagnostic value of gadoxetic acid-enhanced magnetic resonance imaging for liver metastasis. Hepatol Res 2016;46:853-61.

17. Vreugdenburg TD, Ma N, Duncan JK, Riitano D, Cameron AL, Maddern GJ. Comparative diagnostic accuracy of hepatocyte-specific gadoxetic acid (Gd-EOB-DTPA) enhanced MR imaging and contrast enhanced CT for the detection of liver metastases: a systematic review and meta-analysis. Int J Colorectal Dis 2016;31:1739-1749.

18. Amikura K, Kobari M, Matsuno S. The time of occurrence of liver metastasis in carcinoma of the pancreas. Int J Pancreatol. 1995;17:139-46.

19. Besa C, Lewis S, Pandharipande PV et al. Hepatocellular carcinoma detection: diagnostic performance of a simulated abbreviated MRI protocol combining diffusion-weighted and T1-weighted imaging at the delayed phase post gadoxetic acid. Abdom Radiol (NY) 2017;42:179-190.

20. Tillman BG, Gorman JD, Hru JM et al. Diagnostic per-lesion performance of a simulated gadoxetate disodium-enhanced abbreviated MRI protocol for hepatocellular carcinoma screening. Clin Radiol 2018;73:485-493.

21. Vietti Violi N, Lewis S, Liao J et al. Gadoxetate-enhanced abbreviated MRI is highly accurate for hepatocellular carcinoma screening. Eur Radiol 2020;30:6003-6013.

22. Whang S, Choi MH, Choi JI, Youn SY, Kim DH, Rha SE. Comparison of diagnostic performance of non-contrast MRI and abbreviated MRI using gadoxetic acid in initially

diagnosed hepatocellular carcinoma patients: a simulation study of surveillance for hepatocellular carcinomas. Eur Radiol 2020;30:4150-4163.

23. Costa EA, Cunha GM, Smorodinsky E et al. Diagnostic Accuracy of Preoperative Gadoxetic Acid-enhanced 3-T MR Imaging for Malignant Liver Lesions by Using Ex Vivo MR Imaging-matched Pathologic Findings as the Reference Standard. Radiology 2015;276:775-86.

24. Vilgrain V, Esvan M, Ronot M, Caumont-Prim A, Aubé C, Chatellier G. A meta-analysis of diffusion-weighted and gadoxetic acid-enhanced MR imaging for the detection of liver metastases. Eur Radiol 2016;26:4595-4615.

25. Kim HJ, Lee SS, Byun JH et al. Incremental value of liver MR imaging in patients with potentially curable colorectal hepatic metastasis detected at CT: a prospective comparison of diffusion-weighted imaging, gadoxetic acid-enhanced MR imaging, and a combination of both MR techniques. Radiology 2015;274:712-22.

26. Park SH, Kim B, Kim SY, et al. Abbreviated MRI with optional multiphasic CT as an alternative to full-sequence MRI: LI-RADS validation in a HCC-screening cohort. Eur Radiol. 2020;30:2302-2311.

27. Sofue K, Tsurusaki M, Tokue H, Arai Y, Sugimura K. Gd-EOB-DTPA-enhanced 3.0 T MR imaging: quantitative and qualitative comparison of hepatocyte-phase images obtained 10 min and 20 min after injection for the detection of liver metastases from colorectal carcinoma. Eur Radiol. 2011;21:2336-43.

28. van Kessel CS, Veldhuis WB, van den Bosch MA, van Leeuwen MS. MR liver imaging with Gd-EOB-DTPA: a delay time of 10 minutes is sufficient for lesion characterisation. Eur Radiol. 2012;22:2153-60.

29. Marion-Audibert AM, Vullierme MP, Ronot M et al. Routine MRI With DWI Sequences to Detect Liver Metastases in Patients With Potentially Resectable Pancreatic

Ductal Carcinoma and Normal Liver CT: A Prospective Multicenter Study. AJR Am J Roentgenol 2018;211:W217-W225.

30. Jeon SK, Lee JM, Joo I et al. Magnetic resonance with diffusion-weighted imaging improves assessment of focal liver lesions in patients with potentially resectable pancreatic cancer on CT. Eur Radiol 2018;28:3484-3493.

Table 1. Computed Tomography Acquisition and Reconstruction Parameters

	Aquilion 64	Aquilion One	Aquilion Precision	SOMATOM Force
Acquisition parameters				
Number of channels	64	320	160	192
Tube voltage (kVp)	120	120	120	120
Detector configuration (mm)	64 × 0.5	80 × 0.5	80 × 0.5	192 × 0.6
Acquisition matrix	512 × 512	512 × 512	512 × 512	512 × 512
Pitch factor	0.641	0.813	0.813	0.6
Rotation time (s)	0.5	0.5	0.5	0.5
Tube current-time product	AEC	AEC	AEC	AEC
Reconstruction parameters				
Reconstruction plane	Axial	Axial	Axial	Axial
Section thickness (mm)	5	5	5	5
Reconstruction interval (mm)	5	5	5	5
Thin-slice reconstruction				
Reconstruction plane	Axial	Axial	Axial	Axial
Section thickness (mm)	0.5	0.5	0.5	0.6
Reconstruction interval (mm)	0.3	0.3	0.3	0.4

Note.− Detector configuration represents number of detector rows times detector collimation. Thin-slice images were reconstructed on pancreatic and portal venous phase images. AEC = automatic exposure control.

Table 2. MRI Acquisition Parameters

	T1-weighted	T2-weighted	Diffusion-weighted	Dynamic contrast	Hepatobiliary phase
Ingenia 3T					
Repetition time (ms)	216	Resp interval	Resp interval	3.3	3.1
Echo time (ms)	1.0/2.3	85	65	1.6	1.5
Flip angle (°)	70	90	90	10	12
Field of view (mm)	360	360	400	360	360
Matrix	224 × 168	256 × 218	112 × 157	256 × 201	288 × 230
Slice thickness/gap (mm)	6/0	6/0	6/0	4/0	4/0
Echo train length	---	14	---	---	---
Parallel acceleration factor	2	2	2.5	1.8	2.6
Signal averages	1	1	2–4	1	1
Acquisition time (min)	15s	2m	6m	15s	16s
Achieva 3T					
Repetition time (ms)	197	Resp interval	Resp interval	2.9	3.0
Echo time (ms)	1.2/2.3	100	62	1.4	1.5
Flip angle (°)	65	90	90	10	15
Field of view (mm)	380	380	380	380	380
Matrix	240 × 168	320 × 256	128 × 128	304 × 198	368 × 294
Slice thickness/gap (mm)	6/0	6/0	6/0	4/0	4/0
Echo train length	---	18	---	---	---
Parallel acceleration factor	1.6	1.6	3	1.6	1.6
Signal averages	1	1	3–4	1	1
Acquisition time (min)	17s	2m48s	3m36s	15s	18s
Titan 3T					
Repetition time (ms)	205	3000	Resp interval	3.2	3.2
Echo time (ms)	1.3/2.5	100	60	1.1	1.1
Flip angle (°)	72	90	90	12	15
Field of view (mm)	350	350	360	350	350
Matrix	320 × 136	368 × 192	160 × 96	320 × 152	272 × 162
Slice thickness/gap (mm)	8/0	8/0	7/1	4/0	4/0
Echo train length	---	21	---	---	---
Parallel acceleration factor	1.8	2	2	2	2
Signal averages	1	1	2	1	1
Acquisition time (min)	17s	45s	3m33s	17s	17s
Achieva 1.5T					
Repetition time (ms)	206	Resp interval	Resp interval	2.6	2.8
Echo time (ms)	2.3/4.6	60	63	1.2	1.3
Flip angle (°)	80	90	90	13	12
Field of view (mm)	340	340	340	340	340
Matrix	240 × 168	256 × 205	112 × 90	224 × 179	256 × 205
Slice thickness/gap (mm)	6/0	6/0	6/0	4/0	4/0
Echo train length	---	20	---	---	---
Parallel acceleration factor	1.8	1.8	2	1.6	2
Signal averages	1	2	2–3	1	1
Acquisition time (min)	16s	2m30s	5m	20s	17s

Table 3. Characteristics of Patients and Liver Metastases

Characteristic	Finding		
Patient			
Number	130		
Age (years)	68.7	± 10.7	[39–89]
Sex			
Men	72	(55.4%)	
Women	58	(44.6%)	
Interval between CT and MRI (days)	9.2	± 8.0	[0–54]
PDAC			
Location			
Head or neck	83	(63.8%)	
Body or tail	47	(36.2%)	
Resectability according to the NCCN guideline			
Resectable	101	(77.7%)	
Borderline resectable	29	(22.3%)	
Liver metastasis			
Number of patients	13	(10.0%)	
Number of metastases	43		
Size (mm)	6.3	± 2.8	[3.1–13.2]
< 10 mm	38	(88.4%)	
≥ 10 mm	5	(11.6%)	
Reference standard			
Histology	7	(16.3%)	
Follow-up imaging	36	(83.7%)	

Note.− Data are summarized as mean ± standard deviation for continuous variables, or as counts (percentage) for categorical variables. Numbers in brackets indicate ranges. PDAC = pancreatic ductal adenocarcinoma, NCCN = national comprehensive cancer network.

Table 4. Per-lesion Diagnostic Performance for the Detection of Liver Metastases in Patients with Pancreatic Ductal Adenocarcinoma

	Image set 1	Image set 2	Image set 3	*P* Value		
	CECT	CECT + aMRI	CECT + sMRI	set 1 vs. 2	set 1 vs. 3	set 2 vs. 3
Reader 1						
FOM	0.602	0.913	0.926	---	---	---
Sensitivity (%)	23.3 (10/43)	83.7 (36/43)	88.4 (38/43)	<.001	<.001	.50
PPV (%)	71.4 (10/14)	87.8 (36/41)	88.4 (38/43)	.21	.20	>.99
Reader 2						
FOM	0.611	0.894	0.877	---	---	---
Sensitivity (%)	25.6 (11/43)	86.0 (37/43)	86.0 (37/43)	<.001	<.001	>.99
PPV (%)	84.6 (11/13)	86.0 (37/43)	77.1 (37/48)	>.99	.72	.30
Reader 3						
FOM	0.614	0.845	0.856	---	---	---
Sensitivity (%)	25.6 (11/43)	74.4 (32/43)	76.7 (33/43)	<.001	<.001	>.99
PPV (%)	73.3 (11/15)	84.2 (32/38)	94.3 (33/35)	.44	.06	.26
Mean						
FOM	0.609	0.884	0.886	<.001	<.001	.96
Sensitivity (%)	24.8 (32/129)	81.4 (105/129)	83.7 (108/129)	<.001	<.001	.51
PPV (%)	76.2 (32/42)	86.1 (105/122)	85.7 (108/126)	.15	.16	>.99

Note.− Numbers in parentheses are raw data. Numbers in brackets indicate 95% confidence intervals of the value. CECT = contrast-enhanced CT, aMRI = abbreviated MRI, sMRI = standard MRI, FOM = figure of merit, PPV = positive predictive value.

Table 5. Per-patient Diagnostic Performance for the Detection of Liver Metastases in Patients with Pancreatic Ductal Adenocarcinoma

	Image set 1	Image set 2	Image set 3	*P* Value		
	CECT	CECT + aMRI	CECT + sMRI	set 1 vs. 2	set 1 vs. 3	set 2 vs. 3
Reader 1						
Sensitivity (%)	30.8 (4/13) [9.1, 61.4]	92.3 (12/13) [64.0, 99.8]	92.3 (12/13) [64.0, 99.8]	.008	.008	N/A
Specificity (%)	96.6 (113/117) [91.5, 99.1]	97.4 (114/117) [92.7, 99.5]	97.4 (114/117) [92.7, 99.5]	>.99	>.99	N/A
PPV (%)	50.0 (4/8) [22.1, 77.9]	80.0 (12/15) [56.4, 92.5]	80.0 (12/15) [56.4, 92.5]	.18	.18	>.99
NPV (%)	92.6 (113/122) [89.7, 94.8]	99.1 (114/115) [94.6, 99.9]	99.1 (114/115) [94.6, 99.9]	.02	.02	>.99
Accuracy (%)	90.0 (117/130) [83.5, 94.6]	96.9 (126/130) [92.3, 99.2]	96.9 (126/130) [92.3, 99.2]	.04	.04	N/A
Reader 2						
Sensitivity (%)	30.8 (4/13) [9.1, 61.4]	84.6 (11/13) [54.6, 98.1]	84.6 (11/13) [54.6, 98.1]	.02	.02	N/A
Specificity (%)	98.3 (115/117) [94.0, 99.8]	98.3 (115/117) [94.0, 99.8]	96.6 (113/117) [91.5, 99.1]	>.99	.63	.50
PPV (%)	66.7 (4/6) [28.8, 90.8]	84.6 (11/13) [57.7, 95.7]	73.3 (11/15) [50.5, 88.1]	.56	>.99	.65
NPV (%)	92.7 (115/124) [89.9, 94.8]	98.3 (115/117) [94.1, 99.5]	98.3 (113/115) [94.0, 99.5]	.06	.06	>.99
Accuracy (%)	91.5 (119/130) [85.4, 95.7]	96.9 (126/130) [92.3, 99.2]	95.4 (124/130) [90.2, 98.3]	.07	.23	.50
Reader 3						
Sensitivity (%)	38.5 (5/13) [13.9, 68.4]	84.6 (11/13) [54.6, 98.1]	84.6 (11/13) [54.6, 98.1]	.03	.03	N/A
Specificity (%)	96.6 (113/117) [91.5, 99.1]	96.6 (113/117) [91.5, 99.1]	98.3 (115/117) [94.0, 99.8]	>.99	.69	.50
PPV (%)	55.6 (5/9) [27.7, 80.3]	73.3 (11/15) [50.5, 88.1]	84.6 (11/13) [57.7, 95.7]	.41	.18	.65
NPV (%)	93.4 (113/121) [90.2, 95.6]	98.3 (113/115) [94.0, 99.5]	98.3 (115/117) [94.1, 99.5]	.10	.10	>.99
Accuracy (%)	90.8 (118/130) [84.4, 95.1]	95.4 (124/130) [90.2, 98.3]	96.9 (126/130) [92.3, 99.2]	.15	.04	.50
Mean						
Sensitivity (%)	33.3 (13/39) [19.1, 50.2]	87.2 (34/39) [72.6, 95.7]	87.2 (34/39) [72.6, 95.7]	<.001	<.001	N/A
Specificity (%)	97.2 (341/351) [94.8, 98.6]	97.4 (342/351) [95.2, 98.8]	97.4 (342/351) [95.2, 98.8]	>.99	>.99	>.99
PPV (%)	56.5 (13/23) [37.9, 73.5]	79.1 (34/43) [66.2, 87.9]	79.1 (34/43) [66.2, 87.9]	.09	.09	>.99
NPV (%)	92.9 (341/367) [91.3, 94.3]	98.6 (342/347) [96.8, 99.4]	98.6 (342/347) [96.8, 99.4]	<.001	<.001	>.99
Accuracy (%)	90.8 (354/390) [87.5, 93.5]	96.4 (376/390) [94.1, 98.0]	96.4 (376/390) [94.1, 98.0]	<.001	<.001	>.99

Note.− Numbers in parentheses are raw data. Numbers in brackets indicate 95% confidence intervals of the value. CECT = contrast-enhanced CT, aMRI = abbreviated MRI, sMRI = standard MRI, PPV = positive predictive value, NPV = negative predictive value, NA = not applicable.

Figure legends:

Figure 1. Flow chart of the study population.

Figure 2. Summary of the lesions detected by each reader. % indicates the percentage of metastases in each category.

Figure 3. A 63-year-old man with pancreatic ductal adenocarcinoma. A 4.4-mm focal lesion is observed in segment 7 (arrows), showing hypoattenuation on contrast-enhanced CT portal venous phase (a), mild hyperintensity on T2-weighted image (b), hyperintensity on diffusion-weighted image (b=1000) (c), hypointensity on hepatobiliary phase (d), and peripheral enhancement on dynamic sequences (e). The lesion was scored 3, 4, and 5 on image sets 1, 2, and 3, respectively, by each reader, and corresponded to a liver metastasis. A hemangioma is observed in segment 8 (arrowhead).

Figure 4. A 78-year-old man with pancreatic ductal adenocarcinoma. A 3.4-mm focal lesion is observed in segment 7 (arrows), showing hypoattenuation on contrast-enhanced CT portal venous phase (a), isointensity on T2-weighted image (b), hyperintensity on diffusion-weighted image (b=1000) (c), hypointensity on hepatobiliary phase (d), and peripheral enhancement on dynamic sequences (e). The lesion was scored 3, 4, and 5 on image sets 1, 2, and 3, respectively, by each reader, and corresponded to a liver metastasis. Another small metastasis is observed near the lesion (arrowhead).

Figure 5. An 86-year-old woman with pancreatic ductal adenocarcinoma. A 5.1-mm focal lesion is observed in segment 6 (arrows), showing hypoattenuation on contrast-enhanced CT portal venous phase (a), hyperintensity on T2-weighted image (b), isointensity on diffusion-

weighted image (b=1000) (c), hypointensity on hepatobiliary phase (d), and no enhancement on dynamic sequences (e). The lesion was scored 3 on set 1 and scored 1 or 2 on sets 2 and 3 by each reader and corresponded to a hepatic cyst.

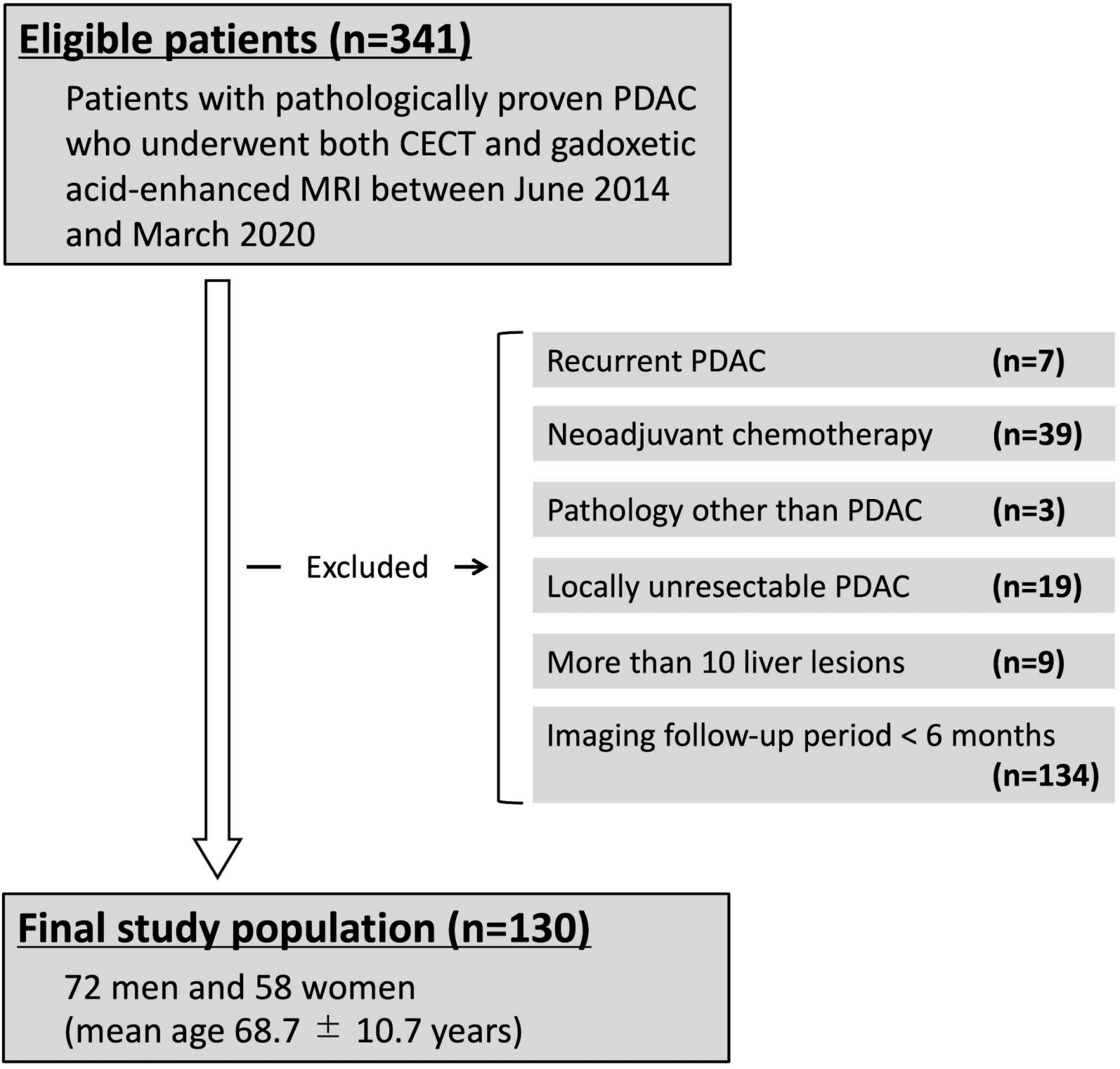
Eligible patients (n=341)
Patients with pathologically proven PDAC who underwent both CECT and gadoxetic acid-enhanced MRI between June 2014 and March 2020
Excluded
Recurrent PDAC (n=7)
Neoadjuvant chemotherapy (n=39)
Pathology other than PDAC (n=3)
Locally unresectable PDAC (n=19)
More than 10 liver lesions (n=9)
Imaging follow-up period < 6 months (n=134)
Final study population (n=130)
72 men and 58 women
(mean age 68.7 ± 10.7 years)

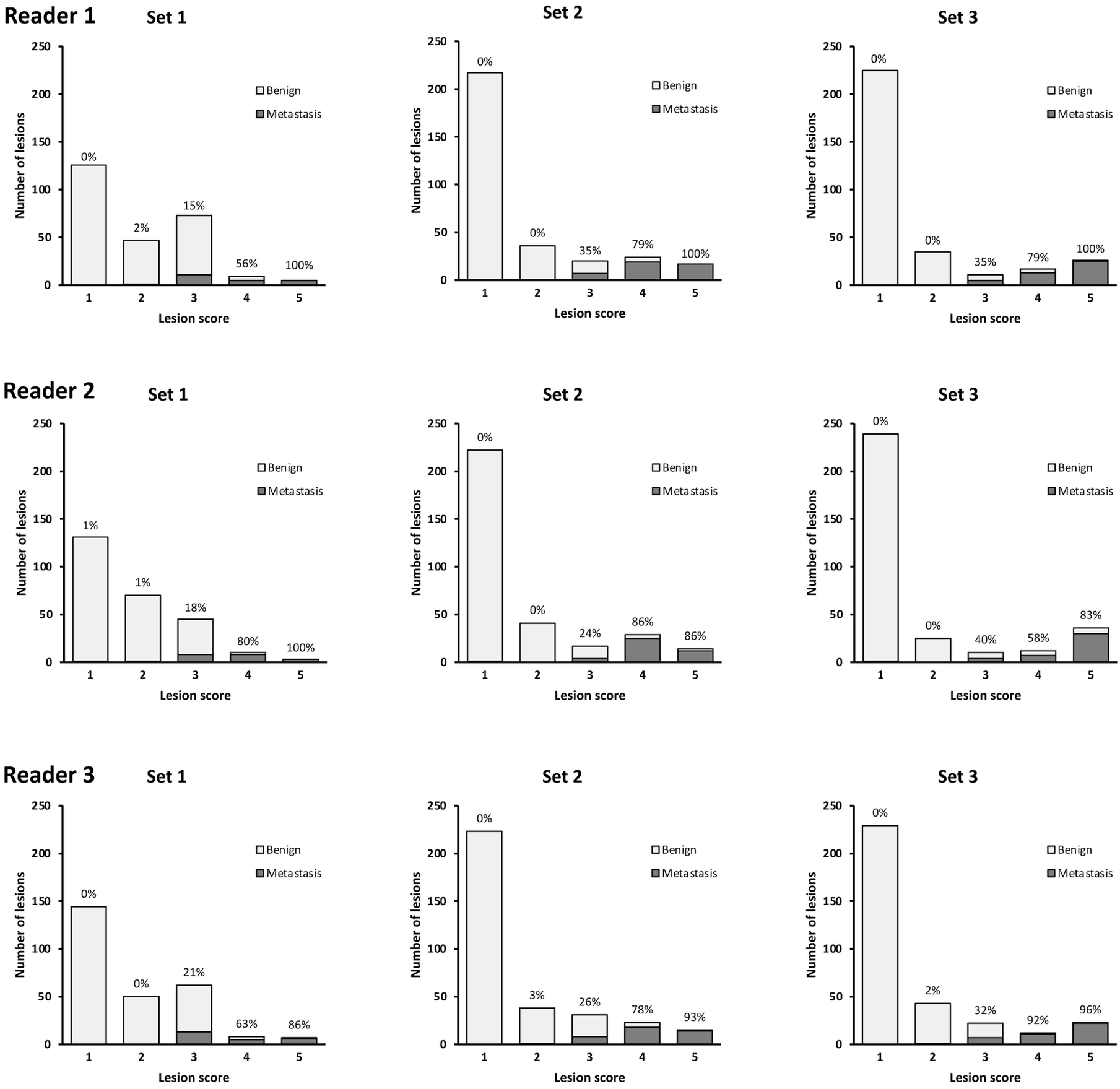
Reader 1
Set 1
Set 2
Set 3
Reader 2
Set 1
Set 2
Set 3
Reader 3
Set 1
Set 2
Set 3
Benign
Metastasis
Number of lesions
Lesion score
0
50
100
150
200
250
1
2
3
4
5
0%
2%
15%
56%
100%
0%
0%
35%
79%
100%
0%
0%
35%
79%
100%
1%
1%
18%
80%
100%
0%
0%
24%
86%
86%
0%
0%
40%
58%
83%
0%
0%
21%
63%
86%
0%
3%
26%
78%
93%
0%
2%
32%
92%
96%

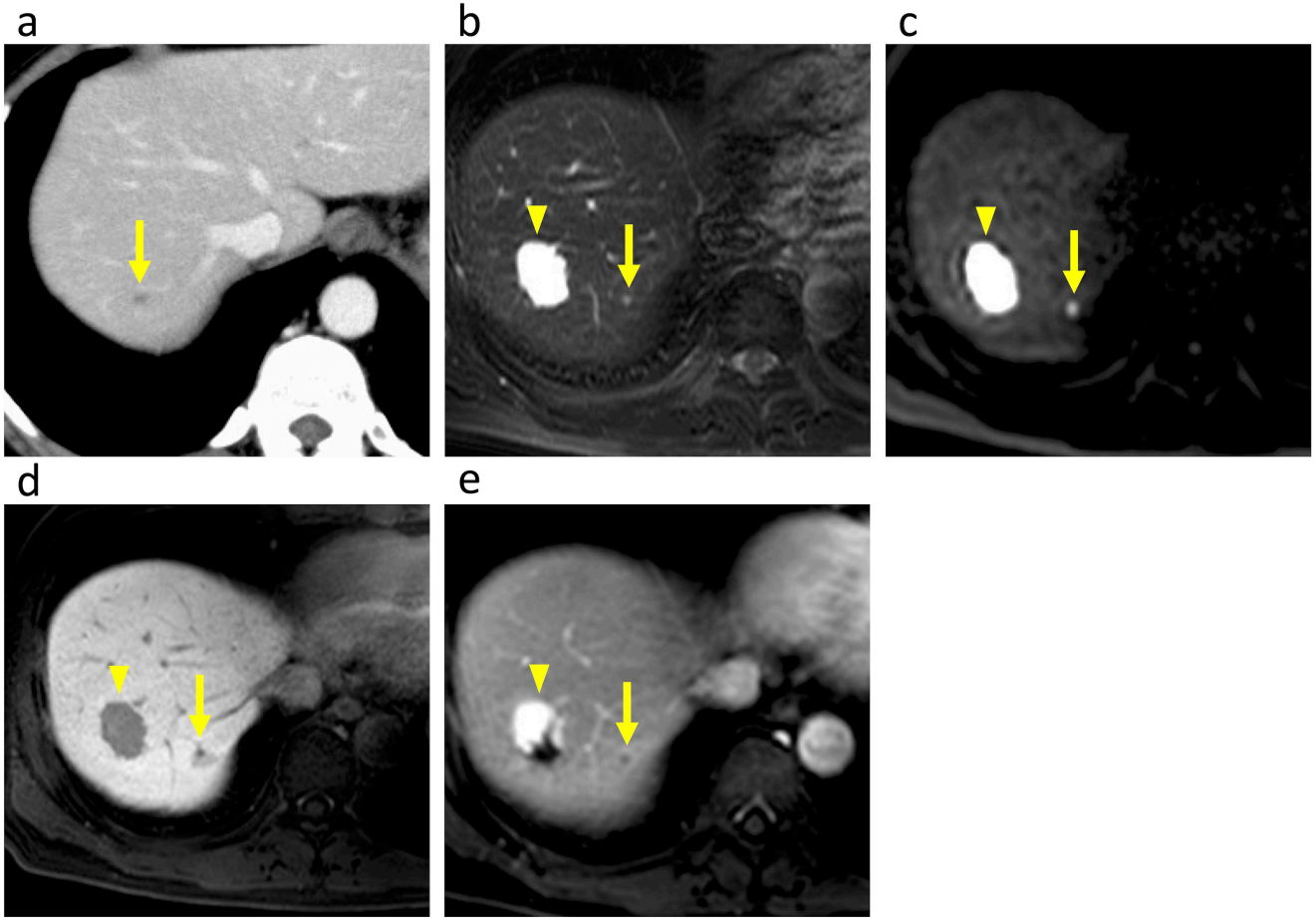
a
b
c
d
e

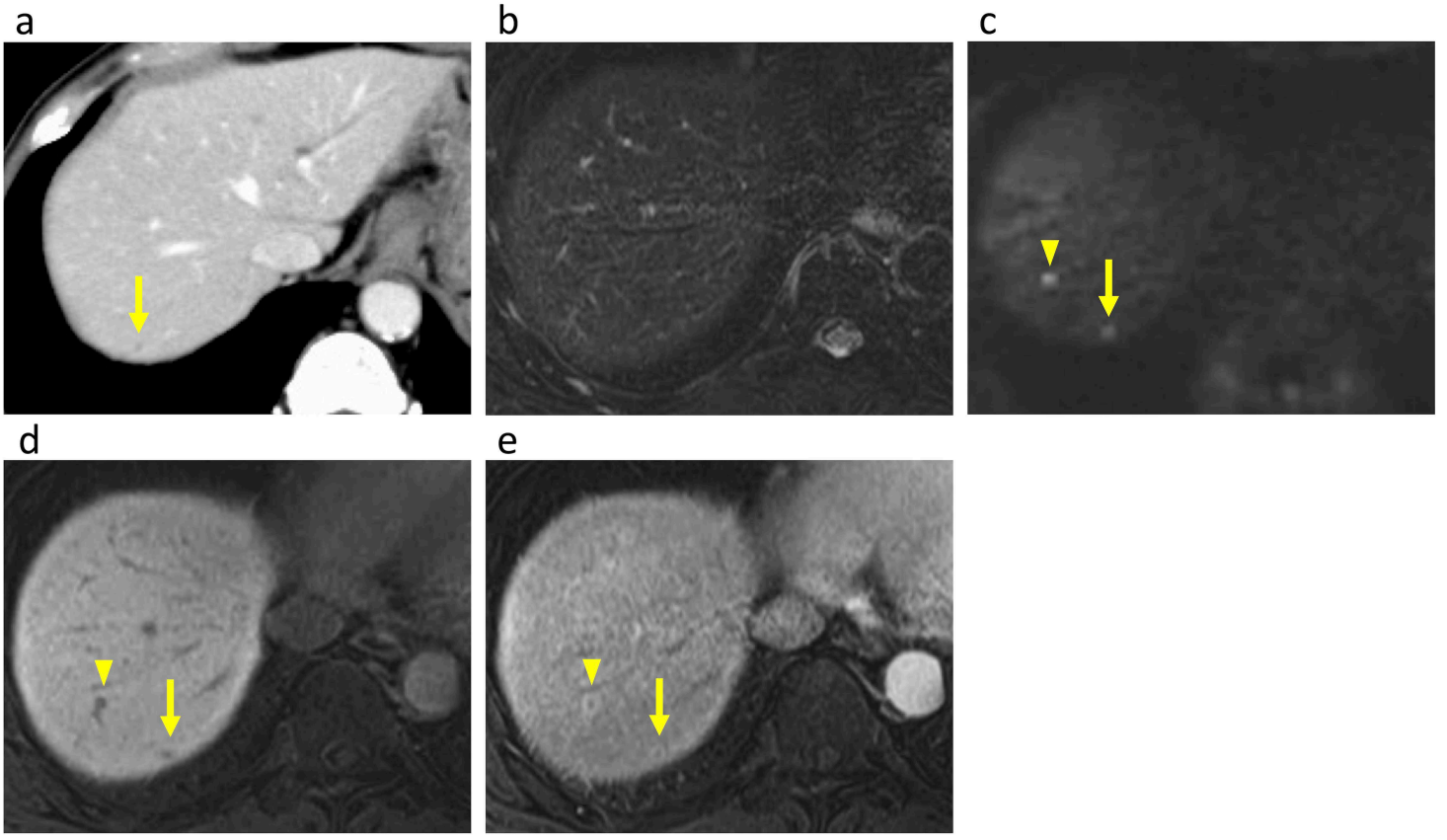
a
b
c
d
e

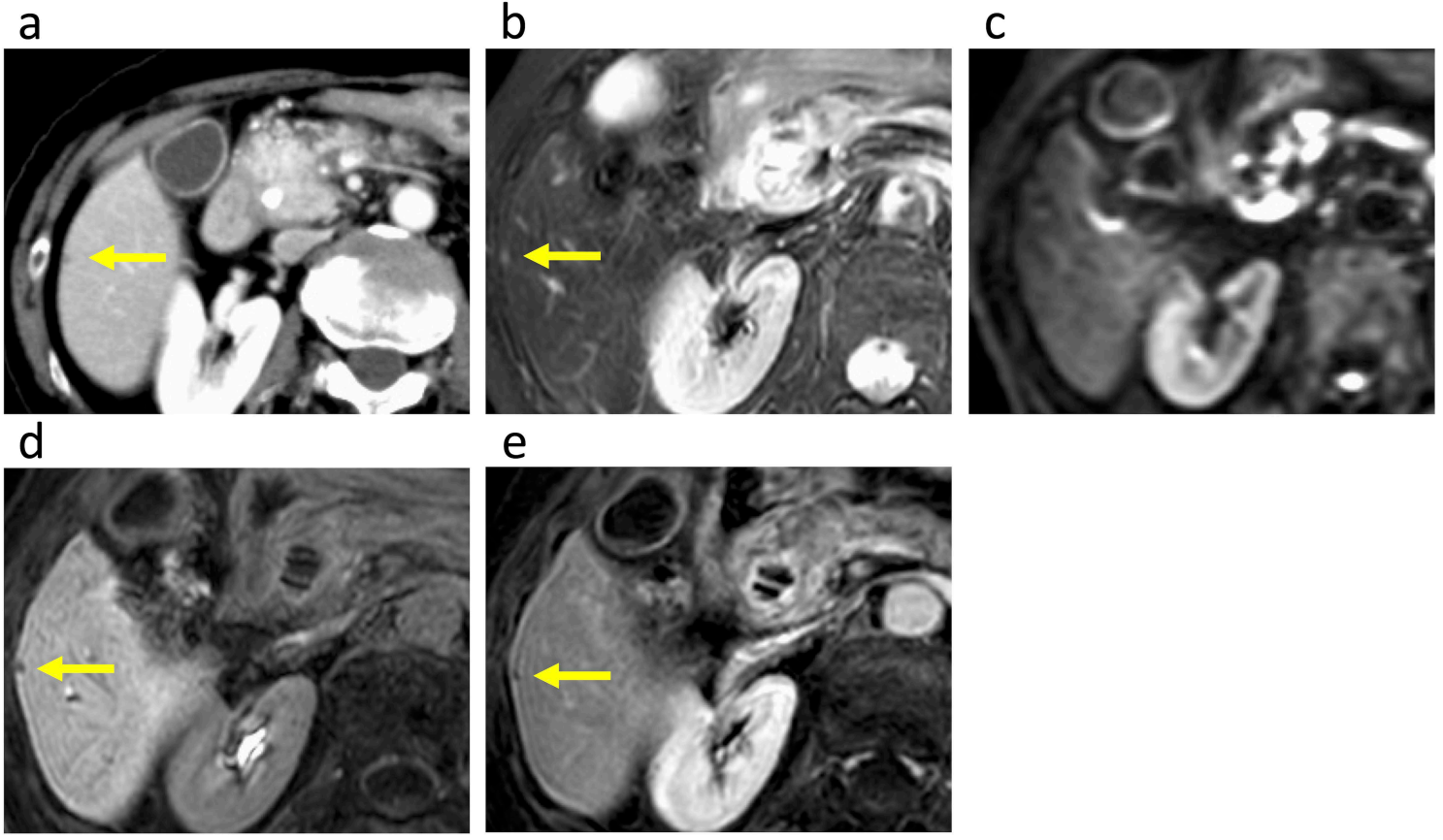
a
b
c
d
e